

A TIME-FREQUENCY BASED MULTIVARIATE PHASE-AMPLITUDE COUPLING MEASURE

Tamanna T. K. Munia and Selin Aviyente

Michigan State University
Department of Electrical and Computer Engineering, East Lansing, MI, 48824, USA
aviyente@egr.msu.edu

ABSTRACT

Interaction of neuronal oscillations across different frequency bands plays an important role in perception, attention, and memory. One particular form of interaction is the modulation of the amplitude of high-frequency oscillations by the phase of low-frequency oscillations, known as phase-amplitude coupling (PAC). Current methods for quantifying PAC mostly rely on Hilbert transform which assumes that brain activity is stationary and narrowband. Moreover, these methods are limited to quantifying bivariate PAC and cannot capture multivariate cross-frequency coupling between different brain regions. This paper presents a new complex time-frequency based high resolution PAC measure and its extension to the multivariate case using PARAFAC (Parallel Factor) model. The proposed approach is evaluated on both simulated and real electroencephalogram (EEG) data.

Index Terms— Phase-Amplitude Coupling, time-frequency distribution, multivariate analysis, PARAFAC, EEG

1. INTRODUCTION

Neuronal oscillations across different frequencies play an important role in motor and cognitive functioning [1, 2]. Many ongoing hypotheses suggest that the coupling across frequencies, known as cross-frequency coupling (CFC), controls multi-scale information processing [3]. The most commonly studied type of CFC looks at the coupling between the amplitude of a high frequency oscillation and the phase of a low frequency oscillation and is known as Phase-Amplitude Coupling (PAC) [4, 5]. PAC between the amplitude of broadband gamma activity (30-100 Hz) and the phase of various low frequency rhythms (typically 5-12 Hz) has been reported across several regions of the brain including the hippocampus, the basal ganglia, and the neocortex [2]. The frequency bands, the magnitude of coupling and the phase involved in PAC vary with time and with anatomical specificity during the execution of different cognitive and sensory tasks [6].

Given the diverse role of PAC in neuronal functioning, there is a need to obtain unbiased, robust estimates of PAC. Existing PAC measures rely on first bandpass filtering the

neuronal oscillations followed by the Hilbert transform to extract phase and amplitude estimates of the oscillations [7]. However, neuronal oscillations are not necessarily narrowband and stationary. Therefore, the quantification of PAC through Hilbert transform may lead to misidentification of CFC [8, 9]. Recently, a generalized Morse wavelets (GMWs) transform based PAC measure have been proposed, but the performance of the method depends largely on the choice of the input frequency range and different design parameters in GMW [10]. Moreover, despite the increasing availability of multichannel recordings like EEG and MEG, these current methods focus solely on the single channel PAC. As indicated by de Cheveigne *et al.*, a single channel recording does not necessarily correspond to a single brain dynamic [11]. Therefore, there is a need for a multivariate PAC measure that can determine cross-frequency interactions across channels.

In this paper, we first describe a new PAC measure based on complex Reduced Interference Distribution (RID)-Rihaczek time-frequency distribution [12]. Unlike the current Hilbert transform based approaches, proposed approach does not require any bandpass filtering and use the properties of the complex time frequency distribution to offer a high-resolution PAC estimate. Moreover, the existing CFC measures are bivariate in nature, focusing on phase amplitude modulations within a channel. In this paper, we extended our PAC measure to quantify multivariate cross-frequency coupling across all channels and frequency bands using an N-way decomposition based on the PARAFAC (Parallel Factor analysis) model. The PARAFAC based multivariate t-f PAC analysis allows us to determine the spatial locations of the amplitude- and phase-providing oscillations as well as to identify the low-high frequency oscillation pairs with significant coupling. The proposed approach is first evaluated on synthesized data and is then applied to multichannel EEG data.

2. BACKGROUND

2.1. RID-Rihaczek Time-Frequency Distribution

For a signal $x(t)$, its RID-Rihaczek distribution is defined as [12]:

$$C(t, f) = \iint \exp\left(-\frac{(\theta\tau)^2}{\sigma}\right) \exp\left(j\frac{\theta\tau}{\sigma}\right) A(\theta, \tau) e^{-j(\theta t + 2\pi f\tau)} d\tau d\theta, \quad (1)$$

where $\exp\left(j\frac{\theta\tau}{\sigma}\right)$ corresponds to the kernel function for the Rihaczek distribution [13], and $\exp\left(-\frac{(\theta\tau)^2}{\sigma}\right)$ corresponds to the Choi-Williams kernel. $A(\theta, \tau)$ is the ambiguity function of the given signal $x(t)$ defined as:

$$A(\theta, \tau) = \int x\left(u + \frac{\tau}{2}\right) x^*\left(u - \frac{\tau}{2}\right) e^{j\theta u} du. \quad (2)$$

This distribution satisfies both the time and frequency marginals. Thus, $\int C(t, f) df = |x(t)|^2$ and $\int C(t, f) dt = |X(f)|^2$.

3. METHODOLOGY

3.1. Time-Frequency PAC (t-f PAC)

PAC between the high frequency (f_a) and low frequency (f_p) oscillations of a given signal is defined as the modulation of the high frequency amplitude, $A_{f_a}(t)$, by the phase of the low frequency, $\phi_{f_p}(t)$. To compute PAC between two neuronal oscillations, $x(t)$ and $y(t)$, where the amplitude of $x(t)$ is modulated by the phase of $y(t)$, first RID-Rihaczek distributions $C_x(t, f)$ and $C_y(t, f)$ are computed as in (1). The amplitude component of $x(t)$ can be computed from the frequency constrained time marginal of $C_x(t, f)$ as follows:

$$A_x^{f_a}(t) = \int_{f_{a_1}}^{f_{a_2}} C_x(t, f) df, \quad (3)$$

where f_{a_1} and f_{a_2} define the bandwidth around the high frequency of interest, f_a . The phase component at the desired frequency f_p for $y(t)$ can be extracted from the complex time-frequency distribution $C_y(t, f)$ as follows:

$$\phi_y^{f_p}(t) = \arg \left[\frac{C_y(t, f_p)}{|C_y(t, f_p)|} \right]. \quad (4)$$

After detecting the amplitude and phase components, the phase-amplitude coupling between the two signals can be computed using the mean vector length (MVL) [14] as follows:

$$MVL_{x,y}(f_p, f_a) = \left| \frac{1}{T} \sum_{t=1}^T A_x^{f_a}(t) e^{j\phi_y^{f_p}(t)} \right|. \quad (5)$$

where T is the number of time points. MVL quantifies the coupling between f_p and f_a by taking the length of the average vector.

3.2. Statistical Significance Testing

A statistical significance test was conducted by comparing individual t-f PAC values with a reference distribution obtained under the null hypothesis that the amplitudes and phases are uncorrelated. Reference distributions were created by generating 100 surrogate data by randomly shuffling the data and

pairing the phase of one trial with the amplitude of another trial. Thus, 100 random MVL values were computed for each electrode and frequency pair. Using these values, a threshold value is obtained for 95% confidence interval. t-f PAC MVL values that surpass the threshold value are considered significant and used for the following multivariate analysis.

3.3. Multivariate t-f PAC (mv t-f PAC)

After computing the pairwise t-f PAC for all N recording sites and across all frequencies of interest, f_p and f_a , a $N \times N$ weighted and directed connectivity network, \mathbf{A}^{f_p, f_a} , where $A_{ij}^{f_p, f_a} = MVL_{i,j}^{f_p, f_a}$ for all $1 \leq i, j \leq N$ is constructed based on the significant pairwise t-f PAC values. Once these adjacency matrices are constructed across different frequency bands, the goal of multivariate analysis is to identify the significant low-frequency and high-frequency phase-amplitude modulation pairs. For this purpose, in this paper we focus on four different low frequency bands (f_{ps}) that may modulate the high frequency amplitude (f_a). To identify the particular components of multivariate PAC, we use PARAFAC decomposition [15].

Given \mathbf{A}^{f_p, f_a} , a 3-way tensor $\mathcal{A} \in R^{N \times N \times K}$ is constructed where $\mathcal{A}(:, :, k)$ corresponds to the k th low frequency band and $K = 4$ in our applications. A 3-way PARAFAC decomposition is used to express \mathcal{A} in terms of its factors across each mode as:

$$\mathcal{A}_{jki} = \sum_{f=1}^F a_{jf} b_{kf} c_{if}, \quad (6)$$

where a_f, b_f, c_f are the loading vectors across each mode and F is the number of components determined by the core-consistency, relative fit and loss parameters described in [16]. a_{fs} provide the spatial loading for the different phase-providing channels whereas b_{fs} provide the spatial loading for the different amplitude-providing channels. The third mode of the tensor \mathcal{A} corresponds to the low and high frequency band pairs that generate significant PAC, so c_{fs} provide the profile for the different PAC frequency pairs.

4. RESULTS

4.1. Multivariate t-f PAC for Synthesized data

4.1.1. Synthesized Data

Synthesized EEG data were generated by creating time series in 2,004 dipole locations in the brain, where the locations were based on a standard MRI brain. Random data were created by computing the inverse Fourier transform of random complex numbers which were sampled from a uniform distribution. As the spectrum of EEG data follows the power law, a sigmoidal curve was tapered on the spectrum of the generated random data to impose a $(1/f)$ shape and then concatenating the mirrored version of the tapered spectrum to generate the

negative frequencies. This procedure was performed individually for each voxel to generate the 2004 uncorrelated dipole positions in the brain. Next, cross-voxel correlations were enforced across all dipoles by generating a random dipole-to-dipole correlation matrix, and calculating the new data as $Y = X^T V D$, where V and D are eigenvectors and eigenvalues of the generated correlation matrix, and X is the data matrix. The forward model for projecting each dipole to the scalp EEG locations were generated following the algorithm developed by openmeeq [17] implemented in Brainstorm [18].

To impose phase-amplitude coupling on the simulated data, dipole positions corresponding to the low frequency phase component and high frequency amplitude components were selected. The low frequency phase signal at f_p was generated as $x_{f_p}(t) = K_{f_p} \sin(2\pi f_p t)$, where K_{f_p} is a fixed scalar that determines the amplitude of the phase frequency (f_p). The high frequency amplitude signal at f_a was generated as $x_{f_a}(t) = A_{f_a}(t) \sin(2\pi f_a t)$, where, $A_{f_a}(t) = K_{f_a} \frac{1 + \text{Re}(e^{j\phi_{f_p}(t)})}{2}$, $K_{f_a} \in [0, 1]$ determines the coupling strength, $\phi_{f_p}(t)$ is the phase of the low frequency phase providing signal. Finally, the time series data from selected dipoles were replaced with $x_{f_p}(t)$ and $x_{f_a}(t)$ for the low frequency and high frequency components, respectively.

4.1.2. Synthesized Data Results

For the analysis, two low frequency phase components were constructed, one in the central cortex at 5 Hz (theta frequency band) and the other in the frontal cortex at 10 Hz (alpha frequency band). The amplitude providing component was generated at the occipital cortex at 70 Hz with its amplitude modulated by the phase of theta and alpha band oscillations. The correlation between theta-gamma was set to be higher (0.8) compared to the correlation between alpha-gamma (0.5). The dipole positions are shown in Fig.1.

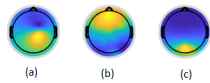


Fig. 1. The dipole locations for the phase and amplitude components used for generating the synthesized data: (a) Theta band (5 Hz) phase providing dipole; (b) Alpha band (10 Hz) phase providing dipole; (c) Gamma band (70 Hz) amplitude providing dipole.

The t-f PAC values for all possible electrode combinations ($N = 64$) were computed and the 64×64 PAC connectivity networks were generated for delta-gamma, theta-gamma, alpha-gamma and beta-gamma bands yielding $\mathcal{A} \in \mathbb{R}^{64 \times 64 \times 4}$. The 3-way PARAFAC decomposition was performed as described in Section 3.3 and the first component of the 3 loading matrices are plotted in Fig.2.

As shown in Fig.2 (a), the spatial profile for the phase providing channels peaks at indices 35 (AFz) and 49 (C6). The amplitude providing channel has a peak at index 28

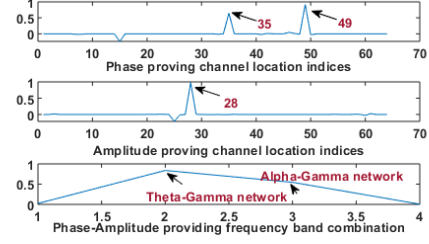


Fig. 2. The PARAFAC decomposition of 3-way tensor \mathcal{A} : (a) Phase providing channel indices; (b) Amplitude providing channel indices; (c) PAC frequency band map.

(POz) (Fig.2 (b)). The PAC frequency band profile in Fig.2 (c) shows that the theta-gamma and alpha-gamma combinations have the highest PAC among the four networks. Fig.3 (a-b) shows the significant edges for these networks with CPz and POz having the highest out-degree and in-degree, respectively. Therefore, these channels are selected as the phase- and amplitude providing channels for theta-gamma band PAC network. Similarly, for alpha-gamma band PAC network, AFz and POz are the phase and amplitude providing channels, respectively. These findings are consistent with the channel combinations detected through PARAFAC decomposition (Fig.2 (a)-(b)) and the dipole positions shown in Fig.1.

The comodulograms are plotted to show the strength of coupling between different oscillation frequencies, by computing the t-f PAC MVL using (5) between the selected pair of electrodes. Fig.3(c) and (d) shows the comodulograms between C6 and POz for theta-gamma network and between AFz and POz for alpha-gamma network, respectively. The proposed multivariate t-f PAC measure can correctly detect the phase (5 Hz and 10 Hz) and amplitude (70 Hz) providing frequencies with a high resolution. Theta-gamma modulation (maximum t-f PAC=0.4523) is also found to be higher than the alpha-gamma modulation (maximum t-f PAC=0.3149).

A comparison of the proposed mv t-f PAC method with the existing Hilbert transform and wavelet transform based PAC method is shown in Fig.3(d) and (g) and Fig.3(e) and (h). It can be seen from Fig. 3(c-f), Fig.3(d-g), and Fig.3(e-h) the proposed multivariate t-f PAC method provides higher resolution estimates of the two frequencies that are coupled with each other compared to the Hilbert transform and wavelet based method. Unlike Hilbert transform based methods, the proposed method does not require bandpass filtering of the signals resulting in high resolution comodulograms.

4.2. Multivariate t-f PAC for EEG data

4.2.1. EEG Data

An EEG dataset from a previously published cognitive control-related error processing study was used to evaluate the proposed PAC measure [19]. The experiment consisted

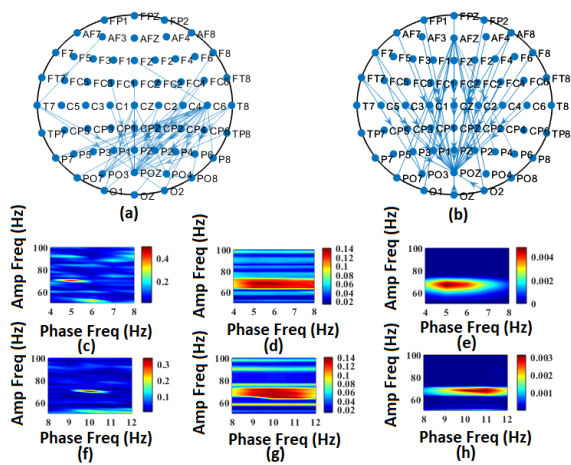


Fig. 3. Directed PAC networks, MV t-f PAC comodulogram, Hilbert transform comodulogram and wavelet transform comodulogram for the significant theta-gamma (a) and alpha-gamma (b) connectivity networks: (a) (b) Directed PAC networks ; (c) (f) MV t-f PAC comodulograms; (d) (g) Hilbert transform comodulograms; (e) (h) Wavelet transform comodulograms

of a letter version of the speeded-reaction Flanker task [20]. A total of 19 participants were considered and the EEG responses were recorded using the 64 electrode ActiveTwo system (BioSemi, Amsterdam, The Netherlands). The data sampled at 512 Hz and averaged over the trials were used for computing the mv t-f PAC.

4.2.2. EEG Data Results

As previous studies indicate increased synchronization associated with the ERN in the time window 25-75 ms [19], mv t-f PAC analysis was performed for the 25-75 ms time window of the EEG data. The t-f PAC values for all possible electrode combinations were computed, and the 64×64 connectivity networks were generated for delta-gamma, theta-gamma, alpha-gamma and beta-gamma band combinations for both error, and correct responses. 3- way tensors were generated for both error and correct responses and the PARAFAC decomposition was performed on both tensors, individually. Fig.4 shows the components for each mode for the two conditions.

As shown in Fig. 4 (c), the theta-gamma frequency modulation network has the highest PAC for both error and correct responses. The theta-gamma PAC network for both error and correct responses are shown in Fig.5 (a) and (b). From Fig. 4, the phase providing channels for error response are FCz, AF7, FT7, FT8, T7, and AF4 and amplitude providing channels are Pz, P2, and POz. Similarly, for the correct response, the phase providing channels were FT8, AFz, and AF8 whereas the amplitude providing channels are C3 and CP3.

The average theta-gamma comodulograms for the two re-

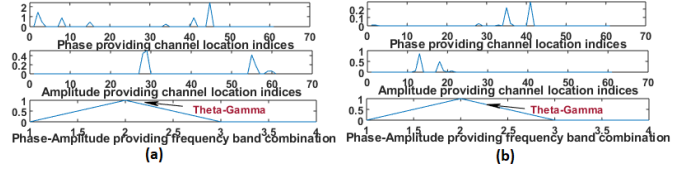


Fig. 4. The PARAFAC decomposition of 3-way tensors \mathcal{A} for error and correct response: (a) error response; (b) correct response.

sponse types are shown Fig.5 (c) and (d). Significantly higher PAC between theta and gamma bands is observed for error response compared to correct response ($p = 0.0079$, Wilcoxon Signed Rank Sum Test with $\alpha=0.05$). This is consistent with prior studies where dynamic PAC was reported between theta phase and gamma amplitude for visual tasks like working memory processing and serial memory recall [7]. Significant theta PAC during error response was also reported in an error processing MEG study [21]. It is hypothesized that large-scale functional integration across different frequency bands supports flexible behavior adaption to improve the performance after an error and thus results in an increase of PAC following error response [22].

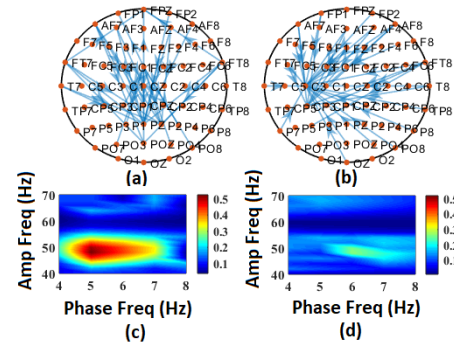


Fig. 5. PAC networks (a-b) and comodulogram (c-d) for the theta-gamma modulation; (a-c) Error response and (b-d) Correct response

5. CONCLUSION

In this paper, we proposed a novel time-frequency based multivariate PAC method for estimating cross-frequency coupling across multichannel recordings using PARAFAC. One limitation is that the computational complexity of the proposed method is $\mathcal{O}(N^2 \log N)$ compared to the complexity of Hilbert transform ($\mathcal{O}(N \log N)$). Despite the higher computational complexity, the proposed method offers higher accuracy and resolution compared to existing methods and offers a framework to detect the frequency diversity along with the spatial distribution of PAC. With these unique properties, proposed measure can lead to the detection of spatially distributed networks which are operating in parallel.

6. REFERENCES

- [1] Gyorgy Buzsaki, *Rhythms of the Brain*, Oxford University Press, 2006.
- [2] Coralie De Hemptinne, Elena S Ryapolova-Webb, Ellen L Air, Paul A Garcia, Kai J Miller, Jeffrey G Ojemann, Jill L Ostrem, Nicholas B Galifianakis, and Philip A Starr, “Exaggerated phase–amplitude coupling in the primary motor cortex in parkinson disease,” *Proceedings of the National Academy of Sciences*, p. 201214546, 2013.
- [3] György Buzsáki, “Neural syntax: cell assemblies, synapse ensembles, and readers,” *Neuron*, vol. 68, no. 3, pp. 362–385, 2010.
- [4] Sampsa Vanhatalo, J Matias Palva, MD Holmes, JW Miller, Juha Voipio, and Kai Kaila, “Infra slow oscillations modulate excitability and interictal epileptic activity in the human cortex during sleep,” *Proceedings of the National Academy of Sciences*, vol. 101, no. 14, pp. 5053–5057, 2004.
- [5] Pascal Fries, “A mechanism for cognitive dynamics: neuronal communication through neuronal coherence,” *Trends in Cognitive Sciences*, vol. 9, no. 10, pp. 474–480, 2005.
- [6] Ryan T Canolty and Robert T Knight, “The functional role of cross-frequency coupling,” *Trends in cognitive sciences*, vol. 14, no. 11, pp. 506–515, 2010.
- [7] Adriano BL Tort, Robert Komorowski, Howard Eichenbaum, and Nancy Kopell, “Measuring phase-amplitude coupling between neuronal oscillations of different frequencies,” *Journal of neurophysiology*, vol. 104, no. 2, pp. 1195–1210, 2010.
- [8] Mark A Kramer, Adriano BL Tort, and Nancy J Kopell, “Sharp edge artifacts and spurious coupling in eeg frequency comodulation measures,” *Journal of neuroscience methods*, vol. 170, no. 2, pp. 352–357, 2008.
- [9] Alexandre Hyafil, “Misidentifications of specific forms of cross-frequency coupling: three warnings,” *Frontiers in neuroscience*, vol. 9, pp. 370, 2015.
- [10] A Nakhnikian, S Ito, LL Dwiell, LM Grasse, GV Rebec, LN Lauridsen, and JM Beggs, “A novel cross-frequency coupling detection method using the generalized morse wavelets,” *Journal of neuroscience methods*, vol. 269, pp. 61–73, 2016.
- [11] Alain de Cheveigné and Lucas C Parra, “Joint decorrelation, a versatile tool for multichannel data analysis,” *Neuroimage*, vol. 98, pp. 487–505, 2014.
- [12] Selin Aviyente and Ali Yener Mutlu, “A time-frequency-based approach to phase and phase synchrony estimation,” *IEEE Transactions on Signal Processing*, vol. 59, no. 7, pp. 3086–3098, 2011.
- [13] August W. Rihaczek, “Signal energy distribution in time and frequency,” *IEEE Transactions on information Theory*, vol. 14, no. 3, pp. 369–374, 1968.
- [14] Ryan T Canolty, Erik Edwards, Sarang S Dalal, Maryam Soltani, Srikantan S Nagarajan, Heidi E Kirsch, Mitchel S Berger, Nicholas M Barbaro, and Robert T Knight, “High gamma power is phase-locked to theta oscillations in human neocortex,” *science*, vol. 313, no. 5793, pp. 1626–1628, 2006.
- [15] Richard A Harshman, “Foundations of the parafac procedure: Models and conditions for an” explanatory” multimodal factor analysis,” 1970.
- [16] Rasmus Bro and Henk AL Kiers, “A new efficient method for determining the number of components in parafac models,” *Journal of Chemometrics: A Journal of the Chemometrics Society*, vol. 17, no. 5, pp. 274–286, 2003.
- [17] Alexandre Gramfort, Théodore Papadopoulo, Emmanuel Olivi, and Maureen Clerc, “Openmeeg: open-source software for quasistatic bioelectromagnetics,” *Biomedical engineering online*, vol. 9, no. 1, pp. 45, 2010.
- [18] François Tadel, Sylvain Baillet, John C Mosher, Dimitrios Pantazis, and Richard M Leahy, “Brainstorm: a user-friendly application for meg/eeeg analysis,” *Computational intelligence and neuroscience*, vol. 2011, pp. 8, 2011.
- [19] Tim P Moran, Ed M Bernat, Selin Aviyente, Hans S Schroder, and Jason S Moser, “Sending mixed signals: worry is associated with enhanced initial error processing but reduced call for subsequent cognitive control,” *Social cognitive and affective neuroscience*, vol. 10, no. 11, pp. 1548–1556, 2015.
- [20] Barbara A Eriksen and Charles W Eriksen, “Effects of noise letters upon the identification of a target letter in a nonsearch task,” *Perception & psychophysics*, vol. 16, no. 1, pp. 143–149, 1974.
- [21] Michael X Cohen and Simon Van Gaal, “Dynamic interactions between large-scale brain networks predict behavioral adaptation after perceptual errors,” *Cerebral Cortex*, vol. 23, no. 5, pp. 1061–1072, 2012.
- [22] Logan T Trujillo and John JB Allen, “Theta eeg dynamics of the error-related negativity,” *Clinical Neurophysiology*, vol. 118, no. 3, pp. 645–668, 2007.